Physics of the Earth and Planetary Interiors 180 (2010) 159–171

Contents lists available at ScienceDirect

Physics of the Earth and Planetary Interiors

journal homepage: www.elsevier.com/locate/pepi

Influence of the crystal field effect on chemical transport in Earth's mantle: Cr^{3+} and Ga^{3+} diffusion in periclase

Katherine L. Crispin[a,*], James A. Van Orman[a,b]

[a] Department of Geological Sciences, Case Western Reserve University, 10900 Euclid Avenue, Cleveland, OH 44106, USA
[b] Department of Chemical Engineering, Case Western Reserve University, 10900 Euclid Avenue, Cleveland, OH 44106, USA

ARTICLE INFO

Article history:
Received 18 May 2009
Received in revised form 3 December 2009
Accepted 21 December 2009

Guest Editors
Kei Hirose
Thorne Lay
David Yuen

Editor
G. Helffrich

Keywords:
MgO
Point defects
Lower mantle
Electronic structure
Transition metal

ABSTRACT

Experiments were performed to determine concentration-dependent diffusion coefficients of Cr^{3+} and Ga^{3+} in periclase at temperatures of 1563–2273 K. Diffusion profiles measured in the quenched samples are consistent with a theoretical model in which the mobile species is a bound M^{3+}-vacancy pair, and each profile was fitted to determine the binding energy and diffusion coefficient of the pair. Trivalent chromium-vacancy pairs diffuse more slowly than Ga^{3+}-vacancy pairs, and with higher migration energy, 237 kJ/mol vs. 190 kJ/mol. Cation vacancies also bind less tightly to Cr^{3+} than to Ga^{3+}, with average binding free energies of −22 and −83 kJ/mol, respectively. At all concentrations and temperatures, Cr^{3+} diffuses much more slowly than Ga^{3+}, by up to two orders of magnitude. The differences between Cr^{3+} and Ga^{3+} cannot be explained by differences in ionic radius or dipole polarizability, but are consistent with the influence of the crystal field on the partially occupied 3d orbitals of Cr^{3+}. The crystal field splitting stabilizes Cr^{3+} on the octahedral cation site, increasing the energy required for Cr^{3+} to exchange positions with an adjacent vacancy. It also makes Cr^{3+}-vacancy pairs less favorable, with the presence of a nearest-neighbor vacancy disrupting the symmetry of the octahedral site, thus diminishing the crystal field stabilization. Trends in the diffusion of first-row divalent transition metals in periclase can also be explained by the crystal field effect. High-spin to low-spin transitions in Fe^{2+}, Co^{2+} or Mn^{2+} would significantly enhance their crystal field stabilization in periclase, and if such spin transitions occur in the deep mantle, they would be expected to slow the diffusivity of these ions significantly, perhaps by several orders of magnitude.

1. Introduction

The physical transport of matter by diffusion is fundamental to many important mantle processes, including chemical and isotopic transfer between minerals and melts (e.g. Hofmann and Hart, 1978; Iwamori, 1992; Qin, 1992; Van Orman et al., 2002), creep deformation associated with mantle convection (e.g. Frost and Ashby, 1982; Ranalli and Fischer, 1984; Karato and Wu, 1993; Evans and Kohlstedt, 1995), homogenization of geochemical heterogeneities (e.g. Hofmann and Hart, 1978; Chakraborty et al., 1999; Kogiso et al., 2004; Holzapfel et al., 2005), the anelastic contribution to seismic attenuation (e.g. Karato, 1993; Jackson et al., 2002), chemical exchange during core formation (e.g. Karato and Murthy, 1997; Rubie et al., 2003; Yoshino and Watson, 2005), electrical conductivity (e.g. Gautason and Muehlenbachs, 1993; Dobson and Brodholt, 2000; Farber et al., 2000; Xu and McCammon, 2002), and grain growth (e.g. Yamazaki et al., 1996; Solomatov et al., 2002). Despite the importance of diffusion in a wide range of mantle processes, data on diffusion in mantle minerals remain fairly sparse, and there are many important elements for which no experimental data yet exist. It is critical to gain an understanding of the basic controls on diffusion in minerals, as this is essential to the development of a rigorous theoretical framework for extrapolating diffusion data to the deep mantle and for predicting diffusion coefficients for ions that have not yet been studied experimentally.

Various ionic properties have been found to influence diffusivity in minerals. Ionic charge usually has a strong influence on diffusion, with a negative correlation between cation charge and diffusivity in many silicate minerals (e.g. Cherniak, 2003; Cherniak and Watson, 2003; Saal and Van Orman, 2004, and references therein) and melts (Hofmann, 1980), but with a positive correlation for strongly ionic minerals such as alkali halides, fluorite, and periclase, in which binding of vacancies to highly charged cations significantly enhances their diffusive transport (Keneshea and Fredericks, 1963; Cherniak et al., 2001; Van Orman et al., 2009). Ionic radius appears to have a strong influence on diffusion in some minerals, consistent with a simple elastic strain model for the diffusion migration energy (e.g. Mullen, 1966; Mortlock, 1968; Van Orman et al., 2001).

* Corresponding author. Tel.: +1 216 368 5046; fax: +1 216 368 3691.
E-mail address: katherine.crispin@case.edu (K.L. Crispin).

0031-9201/$ – see front matter © 2009 Elsevier B.V. All rights reserved.
doi:10.1016/j.pepi.2009.12.004

The dipole polarizability of an ion also may influence its diffusivity, and has been suggested to be an important factor determining the diffusivity of divalent transition metals in periclase (Wuensch and Vasilos, 1962).

A parameter that has received little attention but may be important for determining the diffusivity of some important transition metals is the crystal field stabilization energy. Transition metal cations with partially filled d orbitals are stabilized on octahedral sites by the crystal field effect (Burns, 1993). This crystal field stabilization may increase the energy barrier for the migration of ions to adjacent vacancies. Batra et al. (1976, 1980) demonstrated that this effect provided a quantitative explanation for the diffusion activation energies of first-row transition metals in AgCl. A similar influence of the crystal field effect on diffusion of first-row transition metals might be expected in oxide and silicate minerals, because, as in AgCl, these cations tend to partition onto octahedrally coordinated sites.

In order to investigate the influence of the crystal field effect on diffusion, ideally the ionic radius, charge and polarizability would be held constant and only the electronic structure of the atom would be varied. This is not possible to do rigorously, because in general all of these parameters are correlated. Fortunately, however, a pair of ions exists, Cr^{3+} and Ga^{3+}, which are virtual twins except for their electronic structure. These two cations have identical charge, nearly identical radii (0.615 Å for Cr^{3+} and 0.62 Å for Ga^{3+} (Shannon, 1976)), and very similar dipole polarizability (1.45 $Å^3$ for Cr^{3+} and 1.50 $Å^3$ for Ga^{3+} (Shannon, 1993)). However, Ga^{3+} has full 3d orbitals and thus exhibits no crystal field effects, while Cr^{3+} has partially filled 3d orbitals and strong crystal field stabilization on octahedral sites, with stabilization energies greater than 200 kJ/mol on octahedral or distorted octahedral sites in a wide range of minerals and glasses (Burns, 1993). This pair of cations thus seems ideal for examining the influence of the crystal field effect on diffusion in minerals.

Here we present experimental data on the diffusion of Cr^{3+} and Ga^{3+} in periclase (MgO) over a wide temperature range, from 1563 to 2273 K. Periclase was chosen for this initial study because it is an important mineral in Earth's deep mantle, is a relatively rapid conductor of cations compared to most silicate minerals, has perfectly octahedral cation sites, and has a simple rock salt structure that is stable over an extremely wide range of conditions. Also, in periclase we can evaluate the influence of the crystal field effect not only on the activation energy for diffusive migration but on the energy of binding to a vacancy, which is also an important control on diffusion rates in periclase (Van Orman et al., 2009). The data presented here suggest that the crystal field effect has a significant influence on both the migration energy and the binding energy, which combined reduce the diffusivity of Cr^{3+} by up to two orders of magnitude relative to Ga^{3+}. These results suggest that the crystal field effect may exert a strong control on diffusion rates of first-row transition metal cations in Earth's mantle, and that pressure-induced spin transitions, which increase the crystal field stabilization energy, may lead to substantial changes in diffusivity with depth in the deep mantle.

2. Experiments

Trivalent cations substituting on cation sites in periclase tend to bind strongly to cation vacancies, forming highly mobile pairs that significantly enhance their diffusive transport (Van Orman et al., 2003, 2009). The experiments reported here were designed to provide information on both the mobility and the binding energy of Cr^{3+}- and Ga^{3+}-vacancy pairs, following methods similar to those used by Van Orman et al. (2009). The diffusion couple in these experiments consists of a nearly pure MgO single crystal surrounded by MgO powder doped with a single trivalent cation at approximately 1 mol%. After the isothermal diffusion anneal the binding energy and diffusion coefficient of the M^{3+}-vacancy pair are determined by numerical fitting of the concentration-dependent diffusion profile to a simple theoretical model for diffusion with M^{3+}-vacancy binding.

2.1. Starting materials

The reported impurity content of the MgO single crystals, purchased from MTI Corp., was Ca ≤ 40 ppm, Al ≤ 15 ppm, Si ≤ 10 ppm, Fe ≤ 50 ppm, Cr ≤ 10 ppm, B ≤ 5 ppm, and C ≤ 10 ppm. These concentrations are low compared to the concentration of the trivalent cation measured along each of the experimental diffusion profiles and thus are not expected to have had a significant influence on the vacancy concentrations, the binding between trivalent cations and vacancies, or the trivalent cation diffusion rates. The purchased MgO crystals were 10 mm × 10 mm × 0.5 mm, mirror polished on top and bottom. Each crystal was cleaved into approximately 1 mm × 1 mm × 0.5 mm pieces and these pieces were annealed in air at 1500 °C for a few days to reduce surface damage that may have resulted from polishing.

Periclase powder doped with trivalent cations was produced through glycine–nitrate sol–gel combustion synthesis (Chick et al., 1990). MgO powder was dissolved into concentrated nitric acid and the trivalent dopant was added as a 10 mg/ml plasma standard solution (Alfa Aesar). Glycine was added to the solution as a complexing agent (and fuel), and the solution was heated on a hot plate until combustion. The powdered residue was collected and placed in a box furnace, in air, at 900 °C for 24 h to burn off carbon and nitrates. The result of this process is a fine periclase powder doped with a specified amount of trivalent cation. Chromium is expected to have been in the trivalent state following the highly oxidizing conditions of these syntheses, as it is predominantly trivalent in periclase even under quite reducing conditions, in the presence of Cr metal (Eeckhout et al., 2007).

2.2. 1-atm experiments

Experiments at atmospheric pressure were performed in air, with the doped periclase powder packed around an MgO single crystal within a small platinum bucket (Fig. 1a) and suspended in a Deltech vertical tube furnace. In each instance, the furnace had been pre-heated to the experimental run temperature, and the sample heated to the run temperature within a few minutes or less. Temperature was measured continuously using a Type B Pt-Rh thermocouple placed adjacent to the diffusion couple, with measured thermal fluctuations less than 2 K. At the conclusion of the run, the sample was quickly lifted from the furnace and allowed to cool in air. The heating and cooling times were small compared to the overall run time of the experiments, which range from 0.5 to 6 h, and thus no correction for diffusion during heating and/or cooling was necessary.

2.3. Piston cylinder experiments

Experiments were performed in the piston cylinder to extend the temperature range (MgO has significant volatility at very high temperatures) and also to evaluate whether there were contact problems between the crystal and the doped powder in the 1 atm experiments. These experiments were performed at 2 GPa using an end-loaded piston cylinder apparatus at the Geophysical Laboratory of the Carnegie Institution of Washington. A sample chamber was drilled out of a solid magnesia rod so that it was centered within the hotspot of the assembly, which used a graphite furnace surrounded by Pyrex and talc as the pressure medium (Fig. 1b).

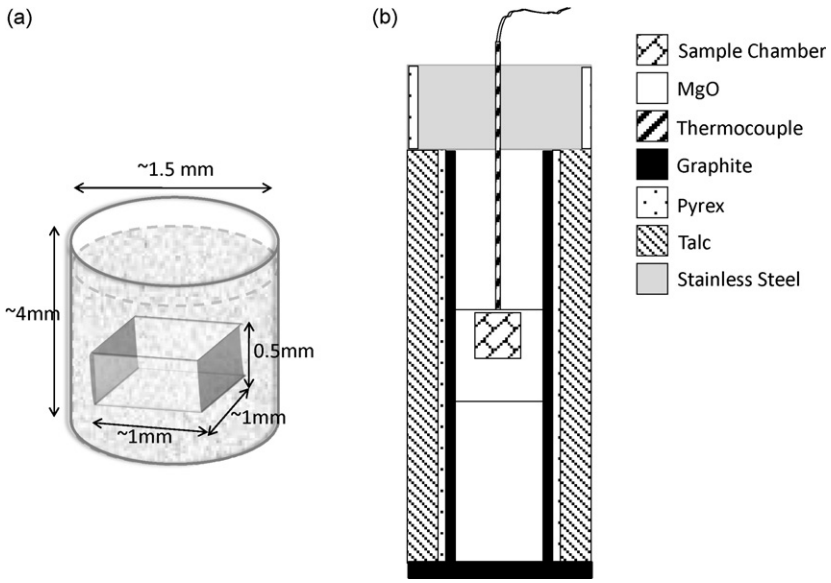

Fig. 1. (a) Schematic illustration of the sample chamber for 1 atm experiments, with approximate dimensions for the sample container and MgO crystal (represented by the rectangular box). The light grey shading represents the doped powder surrounding the crystal. (b) Schematic illustration of a piston cylinder sample assembly. The sample chamber contains an MgO crystal surrounded by doped MgO powder.

Again, a pure MgO single crystal was surrounded by doped MgO powder in sufficient abundance to provide an effectively infinite reservoir of the trivalent cation. A W5% Re/W26% Re thermocouple was inserted into the assembly, resting within 1–2 mm of the single crystal-doped powder interfaces. In this configuration, the temperature variation across the sample should be ~25 K or less (Watson et al., 2002). The samples were heated at a rate of 100 K/min and quenched by shutting off the power. With the exception of Ga^{3+} runs performed at very high temperatures (>2200 K), diffusion during heating and cooling was again considered insignificant compared to the run times, which ranged from 0.25 to 24 h. The procedure used to estimate and correct for diffusion that occurred during heating of the very high-temperature Ga^{3+} experiments is described below.

Samples retrieved from the high-pressure experiments consisted of a poly-crystal/single-crystal diffusion couple, whereas samples retrieved from the 1 atm experiments consisted of the single crystal with, in some cases, powder adhering to the surface (Fig. 2a). In all cases, retrieved samples were mounted in epoxy and ground down approximately 300 μm perpendicular to the diffusion interface. These samples were then polished with diamond suspensions down to 0.25 μm and coated with a thin layer of carbon for electron microprobe analysis.

2.4. Analyses

Diffusion profiles were measured with a JEOL 8900 electron microprobe at the Geophysical Laboratory using an accelerating voltage of 15 kV and a probe current of 50 nA. Standards used were pure MgO for Mg, Ddiopside for Cr, and GaP for Ga. Linear profiles were obtained perpendicular to the edge of the polished surface that was in contact with the doped powder (Fig. 2b). Data collection spots were spaced 2.5–10 μm apart along each profile to ensure no significant overlap. All profiles extended less than 200 μm into the crystal (i.e. they did not reach the center), so that diffusion could be considered one-dimensional, within an effectively semi-infinite medium. Multiple profiles were measured at different locations on each sample to evaluate the internal reproducibility, and several experiments were performed at the same conditions for different times to evaluate the reproducibility between runs.

2.5. Determination of pair diffusion coefficients and binding energies

Van Orman et al. (2009) derived an expression for the diffusion coefficient of a trivalent cation in MgO as a function of its concentration, its binding energy to adjacent vacancies, and the diffusion coefficient of the M^{3+}-vacancy pair:

$$D_{M^{3+}} = D_{\text{pair}} \left\{ \frac{3}{4} - \left(\frac{x_{M^{3+}}^2}{16} + \frac{x_{M^{3+}}}{16\exp(-G_b/RT)} + \frac{1}{576\exp(-2G_b/RT)} \right)^{-1/2} \left(\frac{x_{M^{3+}}}{16} + \frac{1}{32\exp(-G_b/RT)} \right) \right\} \quad (1)$$

where $D_{M^{3+}}$ is the diffusion coefficient of the trivalent cation at a particular concentration, D_{pair} is the diffusion coefficient of the bound trivalent cation/vacancy pair, $x_{M^{3+}}$ is the fraction of cation sites occupied by trivalent cations, and G_b is the Gibbs free energy of association between the trivalent cation and a cation vacancy on a nearest-neighbor site (referred to here as the binding energy). Eq. (1) is based on the theory developed by Lidiard (1955) for divalent cations diffusing in alkali halide crystals, with strong binding between the divalent cations and cation vacancies, and extended by Perkins and Rapp (1973) to the diffusion of trivalent cations in a divalent metal oxide with the rocksalt structure. Its derivation is discussed in Van Orman et al. (2009). Because the diffusion geometry in the experiments reported here was effectively infinite and one-dimensional, the concentration at the single-crystal/polycrystal interface and the concentrations far from the interface on either side remain constant throughout the experiment. With these concentrations fixed, a theoretical diffusion profile based on Eq. (1) can be calculated numerically for given values of the pair diffusion coefficient, binding energy and time. The numerical method involves an iterative solution to the Boltzmann–Matano equation, and is discussed in Van Orman et al. (2009).

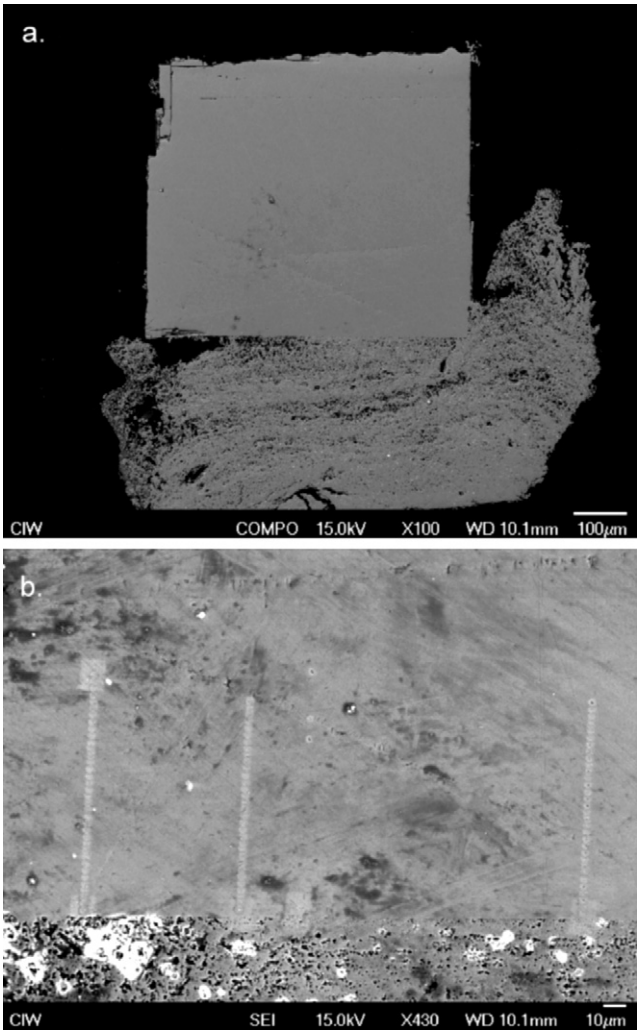

Fig. 2. (a) Back-scattered electron image of a 1 atm experimental sample (Ga070912C) at 100× magnification. The rectangle is the MgO single crystal and the grainy area at the bottom is the doped powder. (b) Secondary electron image showing a close-up of the MgO/powder interface on the same sample. The three lines visible adjacent to the powder, perpendicular to the interface, are the tracks of the electron microprobe analyses of the diffusion profile.

The values of the binding energy and pair diffusion coefficient that best fit each experimental diffusion profile were determined by Chi-square minimization. In fitting the profiles, the concentrations at the interface and at infinite distance were allowed to vary along with the binding energy and pair diffusivity. In this 4-parameter space, in which some of the variables are highly correlated, a robust method was needed to search the 4-parameter space for the minimum of Chi-square. A genetic algorithm was used to narrow down the parameter space, followed by a gradient method to establish the best fit for each of the profiles. This two-step process was necessary because the gradient method became efficient only when the parameter space had been narrowed down significantly using the genetic algorithm.

Several isothermal time series were conducted, two of which are shown in Figs. 3 and 4. Reproducibility among the experiments in the time series can be demonstrated by plotting the concentration profiles with distance scaled by the square root of the run duration (Figs. 3b and 4b). When plotted this way, the diffusion profile should remain invariant with time, regardless of the concentration dependence of the diffusion coefficient. The sqrt(t)-normalized profiles indeed fall within a narrow band in each time series, and the pair diffusion coefficients and binding energies determined from the experiments are generally in good agreement, within the uncertainties determined from analyses of different diffusion profiles from the same experiment.

Gallium diffuses quite rapidly at high temperatures and, at 2273 K, diffusion during heating of the experimental samples was significant. To evaluate and correct for diffusion during heating, a time series was conducted that included a "zero-time" experiment in which the sample was heated as normal, at 100 K/min, but immediately quenched upon reaching 2273 K. The concentration profile measured in this experiment was plotted (Fig. 4) along with the other experimental diffusion profiles from the same temperature as concentration vs. $x/\mathrm{sqrt}(t+t_o)$, where t is the duration of the diffusion experiment and t_o represents the "effective" diffusion time represented by the zero-time profile (i.e. the time at 2273 K that would produce the same diffusion profile). The value of t_o was adjusted to maximize overlap among the concentration profiles on the plot of concentration vs. $x/\mathrm{sqrt}(t+t_o)$, yielding a best-fitting value for t_o of 60 s, which seems quite reasonable considering the heating rate of 100 K/min. Accordingly, 60 s was added to the run duration for calculation of each of the 2273 K Ga^{3+} experiments.

Examples of fitted profiles for both Ga^{3+} and Cr^{3+}, along with their respective inverse error function plots, are shown in Fig. 5.

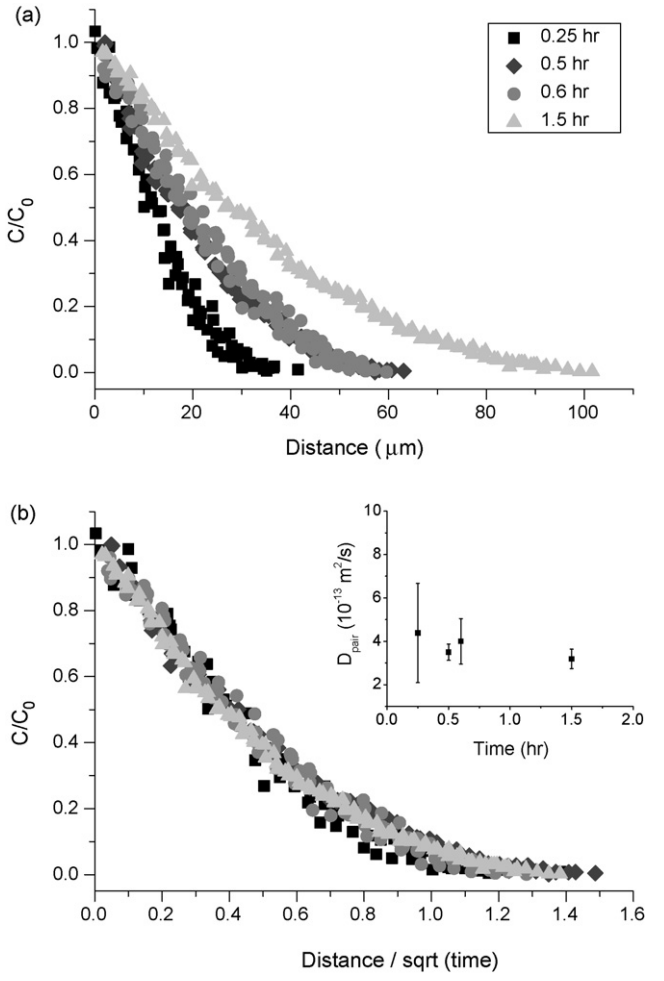

Fig. 3. Results of a time series for Ga at ~1773 K. The 0.6 h experiment was performed at 2 GPa; all other experiments shown here were performed at atmospheric pressure. In (a) diffusion profiles are shown as normalized concentration versus distance (in μm) from the interface. In (b) the same diffusion profiles are shown with distance from the interface (in μm) scaled by the square root of the run duration (in seconds). All profiles overlap within a narrow band, consistent with transport by volume diffusion. The inset graph in (b) shows the pair diffusion coefficient, with 2σ error, determined for each experiment.

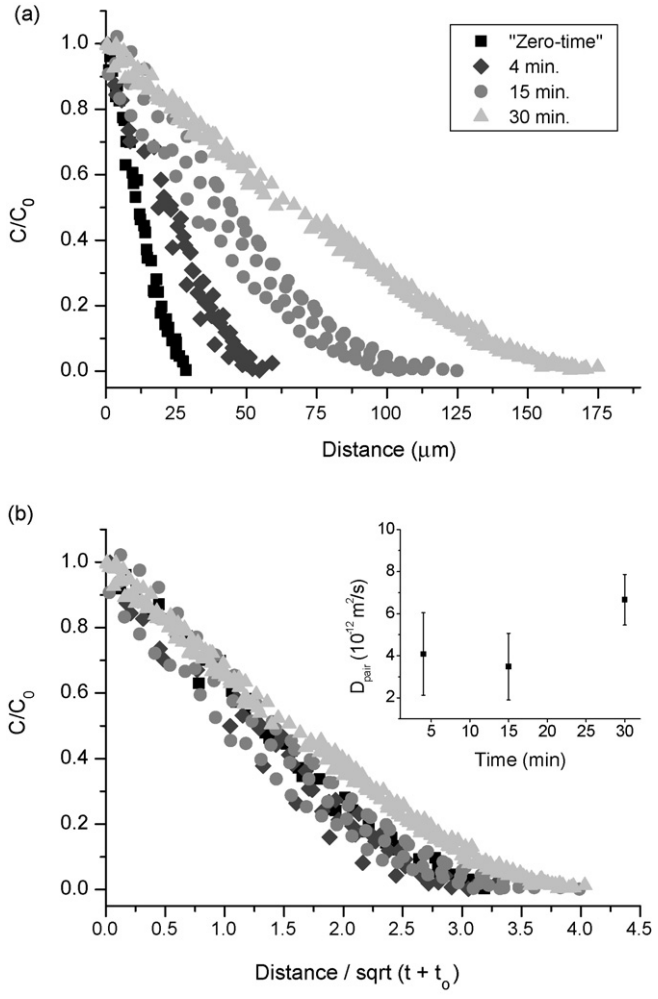

Fig. 4. Results of a time series for Ga at 2273 K and 2 GPa. (a) Normalized concentration versus distance (in μm) from the interface. In (b) the distance from the interface (in μm) is scaled by the square root of the run time (in seconds) plus an effective time t_o that accounts for diffusion that occurred during heating of the sample to the run temperature. The optimum value of t_o (60 s) was chosen to maximize the overlap of the profiles on the plot shown in (b), including a profile from a "zero-time" experiment in which the sample was quenched immediately upon reaching 2273 K. The inset graph in (b) shows the pair diffusion coefficient, with 2σ error, determined for each experiment.

Both experiments were conducted under identical conditions of 1873 K and 2 GPa; however, the Cr^{3+} experiment, with a run duration four times longer, resulted in a shorter profile, slower pair diffusivity and lower binding energy. The concave-up curvature of the profile, plotted as the inverse error function of the normalized concentration vs. distance (Fig. 5b and d), indicates that the diffusion coefficient decreases with decreasing concentration; if diffusion were independent of concentration, the inverse error function profile would be linear on this plot. Note that on the Ga^{3+} inverse error function plot, this curvature is less pronounced, coinciding with a higher binding energy, and lower dependence of diffusivity on concentration over most of the measured profile.

3. Results

Values of the diffusion coefficients for the vacancy-trivalent cation pair, D_{pair}, and the Gibbs free energy of binding (binding energy) of the pair, G_b, along with their respective errors, are given in Table 1 (for Cr^{3+}) and Table 2 (for Ga^{3+}). The values listed in the table are the averages from between 3 and 7 separate diffusion profiles from each experiment, measured at different locations on the crystal. The errors represent two standard deviations.

Table 1
Experimental conditions and results for Cr^{3+}.

Experiment	P (Pa)	T (K)	Time (h)	D_{pair} (10^{-13} m^2/s)	G_b (kJ/mol)
Cr070917	2.0e9	1573	24	0.061 (0.021)	−15.3 (5.5)
Cr071015A	2.0e9	1873	1	1.01 (0.48)	−27.2 (4.7)
Cr070920	2.0e9	1873	4	1.66 (0.92)	−32.1 (17.9)
Cr070919	2.0e9	1873	18	1.36 (0.83)	−21.2 (2.3)
Cr071009	2.0e9	2073	2	3.65 (0.44)	−17.6 (2.0)
Cr071015B	2.0e9	2273	0.5	19.1 (0.79)	−17.1 (2.2)

Table 2
Experimental conditions and results for Ga^{3+}.

Experiment	P (Pa)	T (K)	Time (h)	D_{pair} (10^{-13} m^2/s)	G_b (kJ/mol)
Ga070913A	1.01e5	1563	6	0.530 (0.13)	−97.7 (14.0)
Ga070914	1.01e5	1678	1.85	1.32 (0.26)	−100.1 (11.2)
Ga070912A	1.01e5	1737	4.43	4.92 (0.85)	−59.6 (6.1)
Ga070912C	1.01e5	1777	0.25	3.19 (0.45)	−98.9 (14.0)
Ga070912B	1.01e5	1782	1.5	3.50 (0.37)	−95.6 (10.8)
Ga060328	1.01e5	1783	0.5	4.00 (1.05)	−76.7 (13.3)
Ga071016B	2.0e9	1773	0.6	4.39 (2.29)	−57.5 (19.0)
Ga071004B	2.0e9	1873	1	6.93 (4.57)	−73.4 (10.7)
Ga071004A	2.0e9	2073	0.33	21.4 (7.12)	−84.7 (26.9)
Ga071009	2.0e9	2273	0.5[a]	66.6 (12.2)	−73.6 (7.9)
Ga071016A	2.0e9	2273	0.25[a]	34.8 (15.9)	−83.8 (29.1)
Ga071015	2.0e9	2273	0.0667[a]	40.8 (19.6)	−93.2 (20.1)

[a]These run times refer to the isothermal anneal and do not include an adjustment to account for diffusion during heating of the sample. As discussed in the text, 60 s was added to the diffusion time for each of the 2273 K runs in fitting the profiles for the pair diffusivity and binding energy.

The Cr^{3+}-vacancy pair binding energies fall in the range of −15 to −32 kJ/mol with an average of −21.8 kJ/mol (Fig. 6). The Ga^{3+}-vacancy pair binding energies fall in the range of −58 to −100 kJ/mol with an average of −82.9 kJ/mol (Fig. 6). Neither Cr^{3+} nor Ga^{3+} show clear signs of temperature dependence in terms of their binding to vacancies, indicating that the entropy of binding is fairly small for each. Linear regression of the binding free energies with temperature gives a binding enthalpy of -33.9 ± 14 (2σ) kJ mol^{-1} and entropy of 7.3 ± 7 (2σ) J mol^{-1} K^{-1} for Cr^{3+}-vacancy pairs. For Ga^{3+}-vacancy pairs, the enthalpy of binding is -86.7 ± 40 (2σ) kJ mol^{-1} and the entropy is 5.1 ± 22 (2σ) J mol^{-1} K^{-1}. The small values of the binding entropy obtained here for Cr^{3+} and Ga^{3+}-vacancy pairs are consistent with the small values obtained for the binding entropy between Fe^{3+} and nearest-neighbor vacancies in MgO, which are in the range of −2 to 21 J mol^{-1} K^{-1} (Gourdin and Kingery, 1979; Yager and Kingery, 1981; Hirsch and Shankland, 1991) The enthalpy of binding between Ga^{3+} and a nearest-neighbor cation vacancy is in good agreement with the value of −82 kJ/mol obtained by Carroll et al. (1988) from shell model calculations using empirical interionic potentials. It is also in reasonable agreement with experimental and theoretical values for Fe^{3+}, which exhibits no crystal field splitting and is similar in radius to Ga^{3+}. Values for the binding enthalpy between Fe^{3+} and cation vacancies in periclase are in the range −82 to −57 kJ/mol (Hirsch and Shankland, 1991, and references therein). The enthalpy for Cr^{3+}-vacancy binding determined here, however, is significantly smaller in magnitude than the calculated value of −84 kJ/mol obtained by Carroll et al. (1988). As discussed below, the difference between the experimental and calculated values for the Cr^{3+}-vacancy binding enthalpy may result from crystal field effects, which were not considered in the Carroll et al. (1988) study.

Fig. 7 shows how the diffusion coefficient varies with concentration at three different temperatures. Each curve represents a solution to Eq. (1). Note that as the concentration increases, the diffusivity approaches an asymptote. At high concentrations a higher

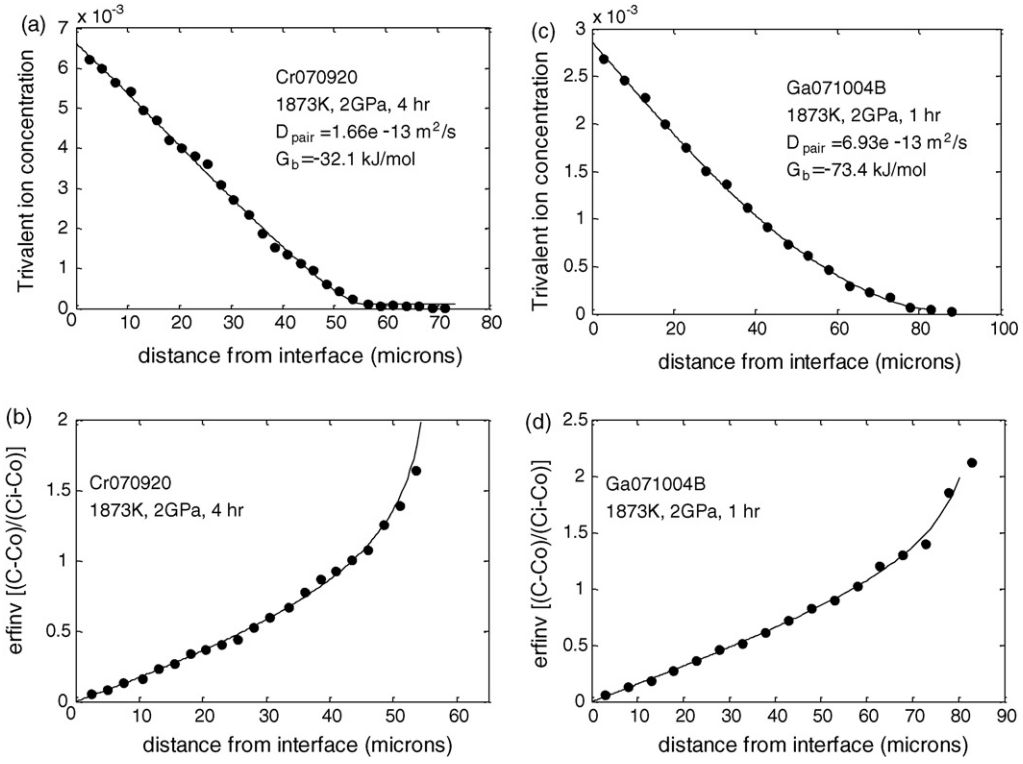

Fig. 5. Typical diffusion profiles and model fits from Cr^{3+} and Ga^{3+} experiments at 1873 K and 2 GPa. (a) Cr diffusion profile from sample Cr070920, with concentration expressed as molar cation fraction. The solid curve represents a numerical solution to Eq. (1). (b) The same Cr diffusion profile shown as the inverse error function of the normalized concentration versus distance. If the diffusion coefficient were independent of concentration, the profile would be linear on this plot. The concave upward curvature indicates that the diffusion coefficient decreases with increasing concentration. (c) Ga diffusion profile from sample Ga071004B, with concentration expressed as molar cation fraction. The solid curve represents a numerical solution to Eq. (1). (d) The same Ga profile shown as inverse error function of the normalized concentration versus distance.

proportion of vacancies are bound to trivalent cations, and when all of the vacancies are bound the diffusivity of the trivalent cation is half the value of the pair. For Ga^{3+} (Fig. 7a), the diffusion coefficient rapidly approaches the asymptote as concentration increases, whereas for Cr^{3+} (Fig. 7b) a significant concentration dependence remains even at relatively high concentrations. This difference in behavior is due to the relatively high binding energy of vacancies to Ga^{3+} compared to Cr^{3+}. The lower binding energy for Cr^{3+} decreases its diffusivity relative to Ga^{3+}, particularly at low concentrations.

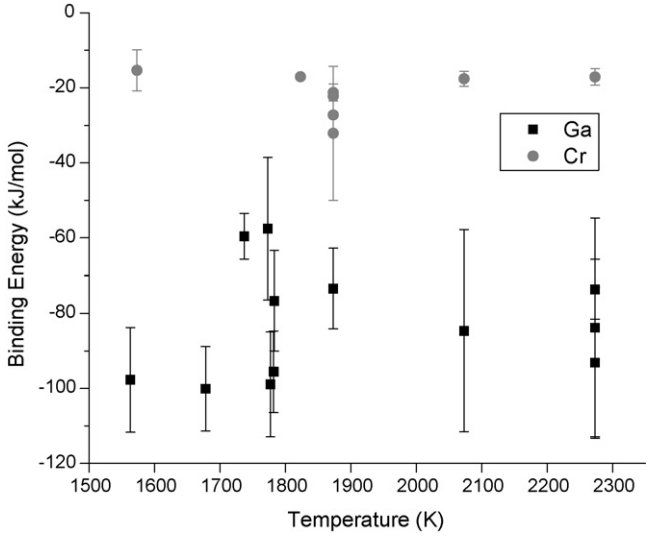

Fig. 6. Gibbs free energy of binding determined from each experiment plotted versus temperature.

The temperature dependence of the trivalent cation-vacancy pair diffusivity is described by the Arrhenius equation:

$$D_{\text{pair}} = D_{\text{o,pair}} \exp\left(\frac{-H_{\text{pair}}}{RT}\right) \quad (2)$$

where D_{pair} is the diffusivity of the pair, R is the gas constant, T is the temperature in Kelvins, and H_{pair} is the activation enthalpy, which, as discussed below, is a composite of the activation enthalpies for Mg-vacancy and M^{3+}-vacancy site exchange. No significant variation in Ga^{3+} diffusivity was determined between experiments performed at 1 atm and 2 GPa, at the same temperatures. This indicates a relatively small activation volume for Ga^{3+}-vacancy pair diffusion, consistent with the activation volume of 3.22 cm^3/mol determined for Al^{3+}-vacancy pair diffusion over a much larger pressure range (Van Orman et al., 2009). Based on the measured activation volume for Al^{3+}-vacancy pair diffusion, a variation in diffusivity of only ~40–50% is expected between 1 atm and 2 GPa, somewhat less than the uncertainty in the measurement of the Ga^{3+}-vacancy pair diffusion coefficient in any experiment. Consistency between the 1 atm and 2 GPa data sets also suggests that there were no significant contact problems in the 1 atm experiments, and that the presence of non-hydrostatic stresses and trace amounts of water had no significant influence on the diffusivities in the piston cylinder experiments. Linear regression (Fig. 8) of the Cr^{3+} pair diffusion data yields an activation enthalpy of 237 ± 11 (2σ) kJ/mol and a pre-exponential factor $\log_{10} D_{\text{pair,o}} = -6.28 \pm 0.56$ (2σ) m^2/s. Linear regression (Fig. 8) of the Ga^{3+} data, including both 1 atm and 2 GPa data sets together, yields an activation enthalpy of 190 ± 13 (2σ) kJ/mol and a pre-exponential factor $\log_{10} D_{\text{pair,o}} = -6.86 \pm 0.74$ (2σ) m^2/s.

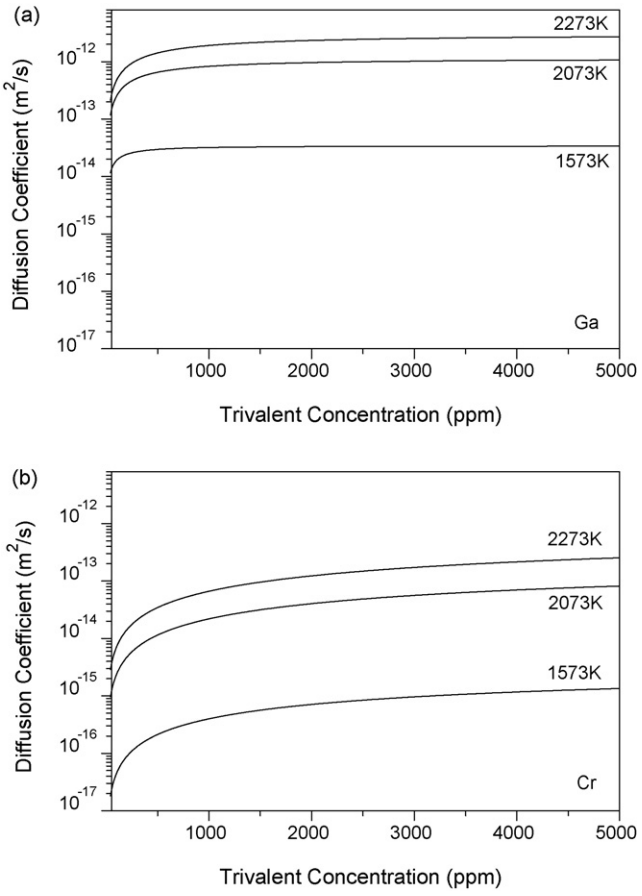

Fig. 7. Diffusion coefficients as functions of concentration at 1573 K, 2073 K, and 2273 K. The curves are solutions to Eq. (1) using the free energy of binding and pair diffusivity determined from experimental diffusion profiles at these temperatures.

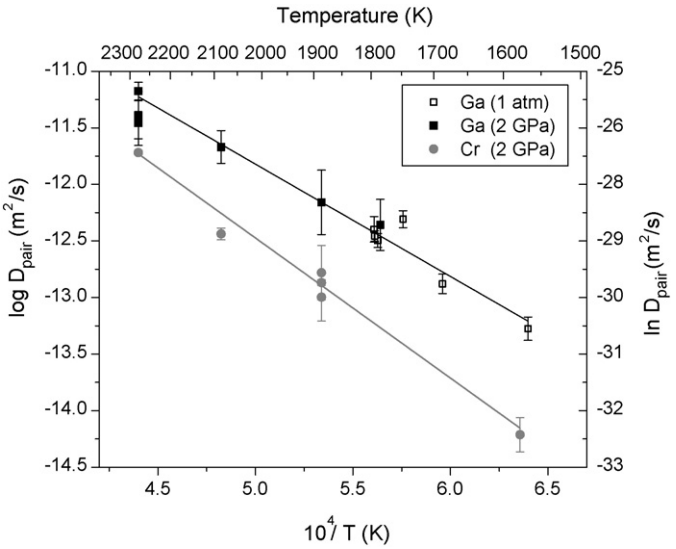

Fig. 8. Arrhenius plot of the Ga^{3+}-vacancy and Cr^{3+}-vacancy pair diffusion coefficients determined from each experiment versus reciprocal temperature.

4. Discussion

4.1. Comparison with prior data on trivalent cation diffusion in MgO

Fig. 9 shows a comparison of previous diffusion data for trivalent cations in periclase with results from the present study. Most of

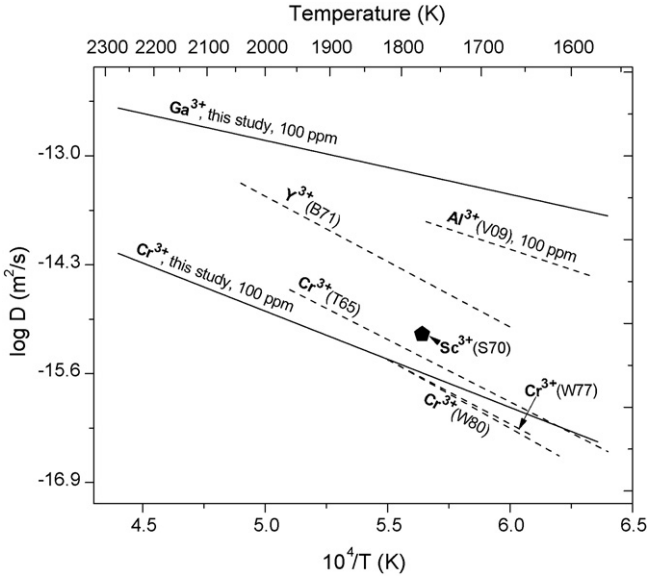

Fig. 9. Summary of diffusion data for trivalent cations in periclase. The data for Cr^{3+} and Ga^{3+} from this study and for Al^{3+} refer to the values at a cation fraction of 100 ppm. All other data shown are from tracer diffusion studies. Sources of data: S70, Solaga and Mortlock (1970); T65, Tagai et al. (1965); W77, Weber et al. (1977); W80, Weber et al. (1980); B71, Berard (1971); and V09, Van Orman et al. (2009).

the data shown are from tracer diffusion studies using high-purity MgO crystals, where the tracer was present at very low concentrations. In general, data on the purity of the crystals used in these experiments are not available, but typical trivalent cation concentrations in high-purity MgO crystals used in diffusion studies in the 1970s are on the order of 100–200 ppm (e.g. Sempolinski and Kingery, 1980). Thus, for the purpose of comparison, the data for Ga^{3+}, Cr^{3+} and Al^{3+} from this study and from Van Orman et al. (2009) are shown at a trivalent cation concentration of 100 ppm, i.e. with a total concentration of extrinsic cation vacancies of 50 ppm. The Cr^{3+} data from this study are in reasonable agreement with the previous tracer diffusion studies, although the activation energy is somewhat smaller.

With the exception of Cr^{3+}, all of the trivalent cations that have been studied in periclase, and are shown in Fig. 9, either have no d electrons or fully occupied d-orbitals, and thus exhibit no crystal field effects. What is striking is that Cr^{3+} is the slowest of these cations, despite having an ionic radius and polarizability nearly identical to Ga^{3+}, the fastest of the trivalent cations that have been investigated in periclase. Because the ionic radii of the other cations cover a wide range, this suggests that the influence of the crystal field effect on the diffusion of Cr^{3+} is quite large compared to the effects of ionic radius.

4.2. Relation of pair diffusion coefficients to site exchange frequencies

There are two different types of jumps that occur during the diffusion of a trivalent cation-vacancy pair. The first is the exchange between the trivalent cation and the attached vacancy, and the second is between the vacancy and other nearest-neighbor Mg sites. Without a site exchange between the vacancy and the Mg sites, long-range diffusion would be impossible since the only movement would be the oscillation between the trivalent cation and the vacancy. The Mg-vacancy exchanges reorient the trivalent cation-vacancy pair so that the trivalent cation can proceed through the lattice. In crystals with the rocksalt structure, such as MgO, the diffusion coefficient of the impurity-vacancy pair is a function of the

Table 3
Enthalpy and entropy of M^{3+}–vacancy binding and site exchange.

	H (kJ/mol)	S (J mol^{-1} K^{-1})
Cr–V binding	−33.9 (14)	7.3 (7)
Ga–V binding	−86.7 (40)	5.1 (22)
Cr–V exchange	238	9.5
Ga–V exchange	182	−2.5

two jump frequencies (Lidiard, 1955):

$$D_{\text{pair}} = \frac{(a/2)^2 \omega_1 \omega_2}{3(\omega_1 + \omega_2)} \tag{3}$$

where a is the lattice parameter (note that in the notation used by Lidiard (1955), a represents half the lattice parameter), ω_1 is the site exchange frequency between the vacancy and any of four equivalent Mg sites surrounding the trivalent cation, and ω_2 is the frequency of the exchange between the vacancy and the trivalent cation. The frequency of exchange between a vacancy and Ga^{3+} or Cr^{3+}, respectively, can be calculated from the experimental pair diffusivity provided that the Mg-vacancy exchange frequency ω_1 is known. Here we assume that ω_1 is equivalent to the Mg-vacancy exchange frequency in the absence of a trivalent cation; this frequency can be extracted from the cation vacancy diffusion coefficients determined from ionic conductivity measurements by Sempolinski and Kingery (1980). The cation vacancy diffusivity is related to the jump Mg-vacancy exchange frequency by the following equation (Balluffi et al., 2005, p. 171, see Eqs. (8.12)–(8.16))

$$D_{\text{V}} = \frac{12\omega_1 r^2}{6} \tag{4}$$

where D_{V} is the vacancy diffusion coefficient, ω_1 is the jump frequency of the vacancy, and r is the jump length. For the rocksalt structure, the jump length for cations, which is equal to the distance between nearest-neighbor cations, is $r = a/\sqrt{2}$, where a is the lattice parameter, 4.211 Å for MgO. Substituting this relationship into Eq. (4) yields the relationship $D_{\text{V}} = \omega_1 a^2$. Using the vacancy diffusion coefficients determined by Sempolinski and Kingery (1980), ω_1 can be determined and then substituted into Eq. (3) to solve for ω_2. What we find for Cr^{3+} is that the frequency of exchange with the attached vacancy is much less than the frequency of exchange between the vacancy and a surrounding Mg atom; $\omega_2 = 0.0473\omega_1$ at 1573 K, and $\omega_2 = 0.0723\omega_1$ at 2273 K. For Ga^{3+} the exchange frequency with the attached vacancy is only slightly smaller than the Mg-vacancy exchange frequency; at 1573 K $\omega_2 = 0.761\omega_1$ and at 2273 K $\omega_2 = 0.271\omega_1$.

The motion entropy and enthalpy of the trivalent impurity can also be calculated (Shewmon, 1989; Balluffi et al., 2005):

$$\omega_1 = \nu \exp\left(\frac{S^{\text{m}}}{R}\right) \exp\left(\frac{-H^{\text{m}}}{RT}\right) \tag{5}$$

where ω_2 is the trivalent cation-vacancy site exchange frequency, S^{m} is the entropy of motion, H^{m} is the enthalpy of motion, and ν is the exchange attempt frequency, approximately equal to the vibrational frequency. For $1/T = 0$, $\omega_{2,0} = \nu \exp(S^{\text{m}}/R)$. Assuming that the exchange attempt frequency for the trivalent cation and vacancy is on the same order as that for Mg^{2+} and vacancy, 1.3e13 s^{-1} (Sempolinski and Kingery, 1980), the motion entropy for Cr^{3+} is calculated to be 9.5 J mol^{-1} K^{-1} and for Ga^{3+} the motion entropy is -2.5 J mol^{-1} K^{-1}. The calculated enthalpies of motion for Cr^{3+} and Ga^{3+} are 238 kJ/mol and 182 kJ/mol, respectively (Table 3).

4.3. Mg diffusion coefficients in Ga^{3+}- or Cr^{3+}-doped periclase

The self-diffusion coefficient of Mg in periclase can be calculated using the equation $D_{\text{mg}} = x_{\text{V}} D_{\text{V}}$, where D_{V} is the vacancy diffusion coefficient and x_{V} is the fraction of vacant cation sites, excluding those that are bound to a trivalent cation. Vacancy diffusivity decreases by about two orders of magnitude when bound to Ga^{3+} or Cr^{3+}, as evidenced by a comparison of the vacancy diffusion coefficients measured by Sempolinski and Kingery (1980) to the pair diffusion coefficients determined in this study (Fig. 8); thus these bound vacancies are not expected to contribute significantly to the transport of Mg under most conditions. The vacancy diffusivity at a particular temperature can be calculated using an Arrhenius equation with a pre-exponential factor of 3.8×10^{-5} m^2/s and activation energy of 220 kJ/mol (Sempolinski and Kingery, 1980). The cation fraction of unbound vacancies can be calculated as $X_{\text{V}} = x_{M^{3+}}(0.5 - p)$, where:

$$p = \frac{3}{4} + \frac{1}{2A} - \sqrt{\frac{1}{16} + \frac{3}{4A} + \frac{1}{4A^2}} \tag{6}$$

and $A = 12 x_{M^{3+}} \exp(-G_{\text{b}}/RT)$ (Van Orman et al., 2009).

Self-diffusion coefficients for Mg were calculated for periclase doped with Ga^{3+} and Cr^{3+}, respectively, at concentrations of 100 ppm, 0.1 mol% and 1 mol%, and are compared with the diffusivity of Ga^{3+} and Cr^{3+} at the same concentrations in Fig. 10. At any given temperature and Ga^{3+} concentration, the Ga^{3+} diffusion coefficient is more than an order of magnitude larger than the Mg^{2+} diffusion coefficient at the same conditions; this difference is magnified at lower temperatures and lower concentrations,

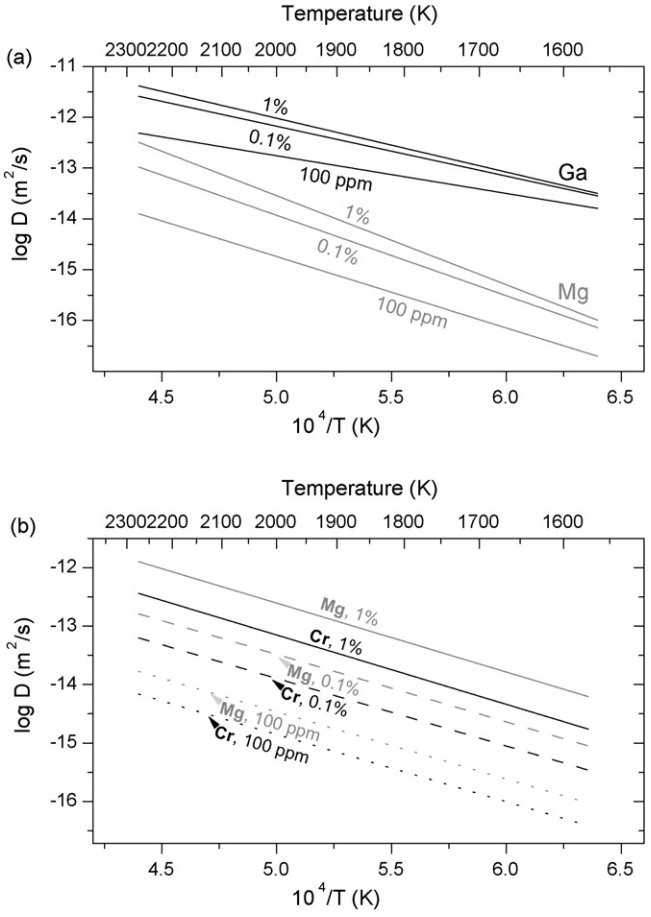

Fig. 10. (a) Calculated diffusion coefficients for Ga (black curves) and Mg (grey curves) plotted versus reciprocal temperature at Ga cation fractions of 100 ppm, 0.1% and 1%. (b) Calculated diffusion coefficients for Cr (black curves) and Mg (grey curves) plotted versus reciprocal temperature at Cr cation fractions of 100 ppm, 0.1% and 1%.

Table 4
Effective activation enthalpies as functions of trivalent cation concentration.

Activation enthalpy (kJ/mol)	Ga	Cr	$Mg_{(Ga)}$[a]	$Mg_{(Cr)}$[b]
M^{3+}-vacancy pair	190	237		
100 ppm M^{3+}	123	217	234	220
0.1% M^{3+}	163	221	263	221
1% M^{3+}	176	227	291	226

[a] Effective activation enthalpy at high temperatures, assuming that Ga is the only trivalent cation present and that the activation enthalpy for cation vacancy diffusion is 220 kJ/mol (Sempolinski and Kingery, 1980).
[b] Effective activation enthalpy at high temperatures, assuming that Cr is the only trivalent cation present.

where the fraction of pairs is larger (Fig. 10a). At high temperatures the fraction of bound pairs decreases, thus Mg^{2+} diffusion is enhanced and Ga^{3+} diffusion is hindered. As a result, the apparent activation energy for Ga^{3+} diffusion is lower than that of the Ga^{3+}-vacancy pair at all concentrations, whereas the apparent activation energy for Mg^{2+} is higher than the Mg^{2+} migration energy (Table 4). For Ga^{3+}, the apparent activation energy becomes small at low Ga^{3+} concentrations, where the fraction of bound pairs is low, and varies significantly with temperature; for Mg^{2+} the apparent activation energy becomes large at high Ga^{3+} concentrations, where the fraction of free vacancies is low and temperature-dependent.

In Cr^{3+}-doped MgO, the calculated Mg self-diffusion coefficients are larger than in Ga^{3+}-doped MgO, due to the weaker binding of cation vacancies to Cr^{3+} and consequently have weaker temperature dependence (Fig. 10b). These result from the smaller binding energy between Cr^{3+} and vacancies; at a given trivalent cation concentration and temperature, the fraction of free vacancies is higher in Cr^{3+}-doped MgO than in Ga^{3+}-doped MgO. While the lower binding energy enhances the diffusivity of Mg in Cr^{3+}-doped crystals, it diminishes the diffusivity of Cr^{3+}. In contrast to Ga^{3+}-doped crystals, where Mg^{2+} is calculated to diffuse more slowly than Ga^{3+} at any temperature and Ga^{3+} concentration, Mg^{2+} is calculated to diffuse faster than Cr^{3+} in Cr^{3+}-doped MgO at any temperature or Cr^{3+} concentration.

4.4. Influence of the crystal field effect on diffusion

Chromium diffuses much more slowly than Ga^{3+} in periclase, has a higher activation enthalpy and binds less tightly to vacancies. An explanation for these differences in terms of ionic radius or dipole polarizability is unlikely, because Ga^{3+} and Cr^{3+} are very similar in these properties; conversely, Al^{3+}, Sc^{3+} and Y^{3+}, for example, have far greater differences in ionic radius and polarizability but smaller differences in diffusivity. The slow diffusivity and weak binding of Cr^{3+} to vacancies likely results from the effect of the crystal field on its partially filled 3d electron orbitals.

Transition metals may contain electrons that occupy two different types of d orbitals that interact differently with the surrounding oxygen anions on octahedral cation sites in periclase (Fig. 11). The three t_{2g} orbitals have less overlap with the six surrounding oxygen anions than the two e_g orbitals, and therefore experience weaker repulsion. Cr^{3+} has three electrons in d-orbitals, and in periclase each occupies one of the lower-energy t_{2g} orbitals. It is a non-spherical cation that fits snugly among the six oxygen anions on the cation site in periclase, thus experiencing significant crystal field stabilization (Burns, 1993). Ga^{3+}, on the other hand, has completely filled d orbitals, two in each of the t_{2g} and e_g orbitals; the lower energy of the three t_{2g} orbitals is cancelled by the higher energy of the two e_g orbitals, and Ga^{3+} therefore experiences no crystal field stabilization.

Fig. 12 shows a schematic of the potential energy surface for a trivalent cation in periclase migrating from a cation site, across a saddle point (assumed here to be the tetrahedrally coordinated interstitial site), into an adjoining vacancy (not shown in the schematic). The energy of the interchange (H_m) between the trivalent cation and the vacancy is equal to the difference in energy when the trivalent cation is on the cation site, and when it is at the interstitial saddle point position. As described in Section 4.2, and listed in Table 3, this energy is calculated from the present experiments as 182 kJ/mol for Ga^{3+} and 238 kJ/mol for Cr^{3+}, indicating that the energy barrier to diffusion is enhanced by ~56 kJ/mol due to the crystal field effect for Cr^{3+}. An upper limit to the enhancement of the energy barrier due to the crystal field effect is the crystal field stabilization energy (CFSE) determined from optical spectroscopy,

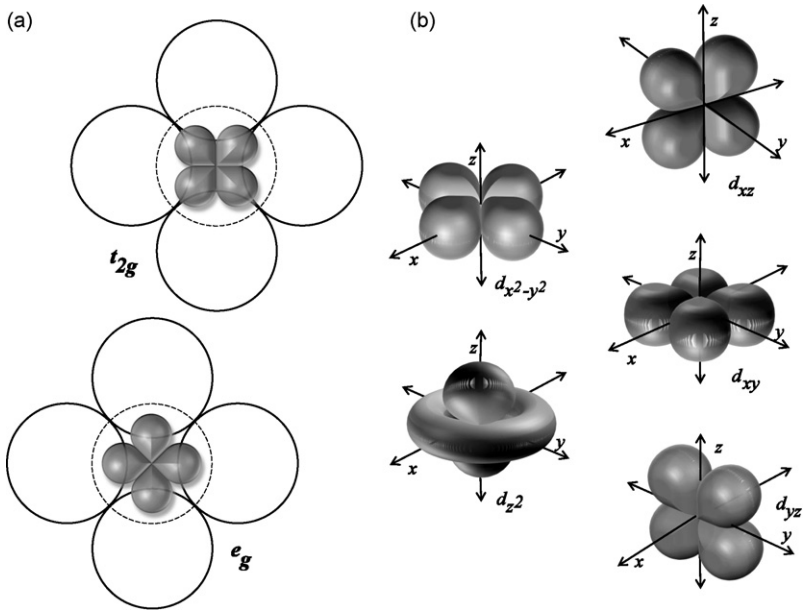

Fig. 11. Schematic representation of d orbitals and their alignment in an octahedral cation site in periclase. Electrons residing in the t_{2g} orbitals (d_{xz}, d_{xy}, and d_{yz}) experience less overlap with the six surrounding oxygen anions than those in the e_g orbitals ($d_{x^2-y^2}$ and d_{z^2}). In (a) the solid and dashed circles represent the positions of the oxygen atoms. In (b) the electron localization surfaces corresponding to the various orbitals are shown without surrounding oxygen atoms.

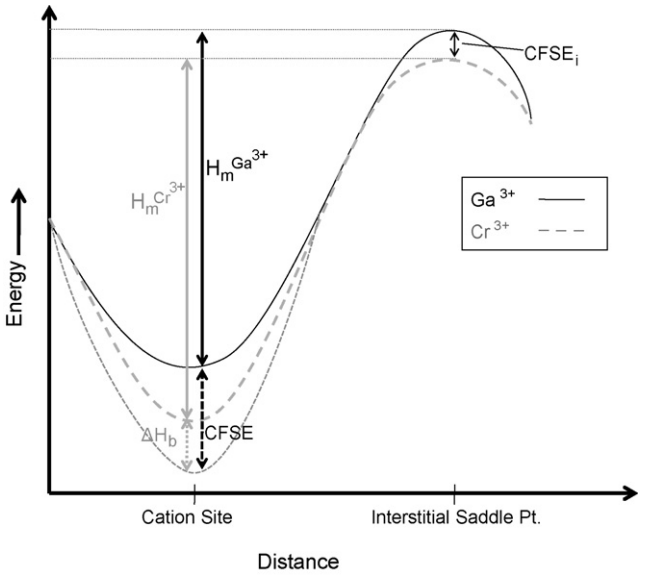

Fig. 12. Schematic representation of the potential energy surface for a trivalent cation between the cation site and the interstitial saddle point along the diffusive jump path. Partially filled d orbitals in Cr^{3+} lower its energy on the cation site relative to Ga^{3+}; when Cr^{3+} is isolated from adjacent vacancies, the lowering of energy on the cation site is equal to the $CFSE_{oct}$ determined from optical absorption spectroscopy. When a cation vacancy is present on an adjacent cation site, as it must be in order for a diffusive jump to occur, the energy well is not as deep as it is when Cr^{3+} is isolated, because there is an energy cost associated with the breaking of octahedral symmetry. The difference between the CFSE of isolated Cr^{3+} and the CFSE of Cr^{3+} with an adjacent cation vacancy is interpreted to be the difference in M^{3+}-vacancy binding enthalpy between Cr^{3+} and Ga^{3+}. The energy at the saddle point along the jump path to an adjacent cation site is also reduced by the crystal field effect for Cr^{3+}. The crystal field stabilization energy at the saddle point is not constrained by optical absorption measurements, but is estimated from the present experiments to be approximately half the value of the CFSE for isolated Cr^{3+} on the cation site in periclase.

which is −232 kJ/mol for Cr^{3+} in periclase (Burns, 1993). This corresponds to the deepening of the energy well on the cation site due to crystal field splitting, and would represent the increase in the energy barrier in the absence of other crystal field effects. However, in addition to an increase in the energy barrier due to the crystal field stabilization on the octahedral site, there is also a reduction in the energy barrier due to the crystal field stabilization of Cr^{3+} at the interstitial saddle point. The CFSE at the interstitial saddle point is expected to be less than that at the octahedral cation site, but still significant. No experimental data exist on the CFSE of Cr^{3+} or any other transition metal on the tetrahedral interstitial site in periclase. In spinels, the CFSE of Cr^{3+} on the tetrahedral site is ∼30% of the value on the octahedral site (Burns, 1993, Table 6.3). The CFSE of Cr^{3+} in the interstitial saddle point configuration in periclase may be somewhat larger, due to the distortion from tetrahedral symmetry induced by the presence of a cation vacancy on either side of the saddle point during the diffusive jump. For ions with $3d^3$ electronic configurations, like Cr^{3+}, distorted sites have lower energy than regular tetrahedral sites (Burns, 1993, p. 36).

The presence of a cation vacancy adjacent to the trivalent cation, which is necessary for a diffusive jump, also disrupts the perfect symmetry of the octahedral cation site. This must reduce the magnitude of the crystal field stabilization because Cr^{3+} prefers perfect octahedral sites (Burns, 1993). The preference of Cr^{3+} for perfectly symmetrical octahedral sites appears to explain why it binds less tightly to vacancies than Ga^{3+}; the presence of a vacancy disrupts the octahedral symmetry and therefore comes with an energy cost. This energy cost can be estimated as the difference in the vacancy binding energy for Ga^{3+} and Cr^{3+}, which is ∼53 kJ/mol (Table 3). The CFSE determined from optical absorption spectroscopy applies to isolated Cr^{3+} with no vacancies in the immediate vicinity (Low, 1957), so does not include this energy cost. Hence, the CFSE relevant to Cr^{3+} diffusion, with a vacancy in the nearest-neighbor cation site, would be −179 kJ/mol rather than −232 kJ/mol. Taking this value for the enhancement of the energy well for Cr^{3+} relative to Ga^{3+}, and the difference in migration energy between Cr^{3+} and Ga^{3+}, we can obtain an estimate for the crystal field stabilization energy of Cr^{3+} in the interstitial saddle point configuration. Following the discussion above, and the schematic potential energy surfaces shown in Fig. 12, the difference in the migration energy (i.e. the vacancy exchange energy) for Cr^{3+} and Ga^{3+} can be written as:

$$(H_m^{Cr^{3+}} - H_m^{Ga^{3+}}) = -CFSE_{oct}^{Cr^{3+}} - (H_b^{Cr^{3+}} - H_b^{Ga^{3+}}) + CFSE_{tet}^{Cr^{3+}} \quad (7)$$

where H_m are the migration enthapies, H_b are the binding enthalpies, and $CFSE_{oct}$ is the crystal field stabilization energy for isolated Cr^{3+} in periclase (with no cation vacancies nearby), and $CFSE_{tet}$ is the crystal field stabilization energy for Cr^{3+} in the saddle point configuration, assumed here to be a tetrahedrally coordinated interstitial position, with a cation vacancy on either side. In writing Eq. (7) we have followed convention in assigning positive values to the migration energies, and negative values to the binding and crystal field stabilization energies. Taking the values from this study for the migration and binding energies, and the value of CFSE for isolated substitutional Cr^{3+} in periclase from Burns (1993), the CFSE for Cr^{3+} in the saddle point configuration is calculated as:

$$CFSE_{tet}^{Cr^{3+}} = (238 - 182) + (-232) + (-34 - (-87)) = -123 \text{ kJ/mol} \quad (8)$$

This is about half the value of the CFSE for Cr^{3+} in perfect octahedral symmetry.

Crystal field effects are likely to be important in the diffusion of other transition metals with partially filled 3d orbitals. To our knowledge, the only previous study that has explicitly considered crystal field effects on the diffusion of transition metals in crystalline solids is a study on first-row divalent transition metals in AgCl (Batra et al., 1976, 1980). In this study, the relative migration energies of the divalent transition metals could be accounted for by consideration of the crystal field stabilization energies in the substitutional and saddle point positions, following an approach similar to that outlined above. Diffusion data for Fe^{2+}, Co^{2+} and Ni^{2+} in periclase from a study by Wuensch and Vasilos (1962) also appear to be consistent with the crystal field exerting a strong influence on diffusion. In this study, a substantial variation in diffusivity was observed among these cations, with Fe^{2+} having the largest diffusion coefficients and smallest activation enthalpy, and Ni^{2+} having the smallest diffusion coefficients and largest activation enthalpy. This trend is the opposite of what would be expected considering ionic radius alone. Fe^{2+} is the largest of the three cations, and Ni^{2+} the smallest; for divalent cations that exhibit no crystal field splitting, diffusion coefficients are usually found to decrease with increasing ionic radius (Mortlock, 1968). The variations in diffusion coefficient and activation energy are, however, consistent with the influence of the crystal field on the energetics of diffusion. Divalent nickel, the slowest of the three cations in the study, has fully occupied t_{2g} orbitals (with six electrons), and half occupied e_g orbitals (two electrons), and a CFSE on octahedral cation sites in periclase of −122.1 kJ/mol (Burns, 1993); Co^{2+}, the next slowest, has one less electron in the t_{2g} orbitals and a CFSE of −86.2 kJ/mol (Burns, 1993); and Fe^{2+}, the fastest of the three cations, has four electrons in t_{2g} orbitals and two in e_g orbitals, and a CFSE of −51.7 kJ/mol (Burns, 1993). Together with the present data on the migration energy of Ga^{3+} and Cr^{3+}, the Wuensch and Vasilos (1962) data on the activation enthalpy of these divalent transition metals correlate rather well with the CFSE on the octahedral cation site (Fig. 13).

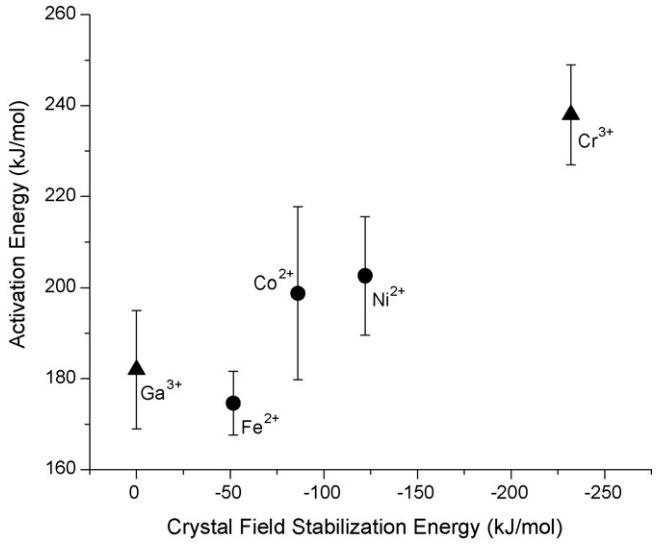

Fig. 13. The activation enthalpy for diffusion is plotted against the crystal field stabilization energy for transition metals in periclase. For Ga^{3+} and Cr^{3+}, the activation energy shown is the enthalpy of exchange with an adjacent vacancy determined from the present experiments. Activation enthalpies for Fe^{2+}, Co^{2+} and Ni^{2+} are the values determined from diffusion experiments by Wuensch and Vasilos (1962). Crystal field stabilization energies are from Burns (1993).

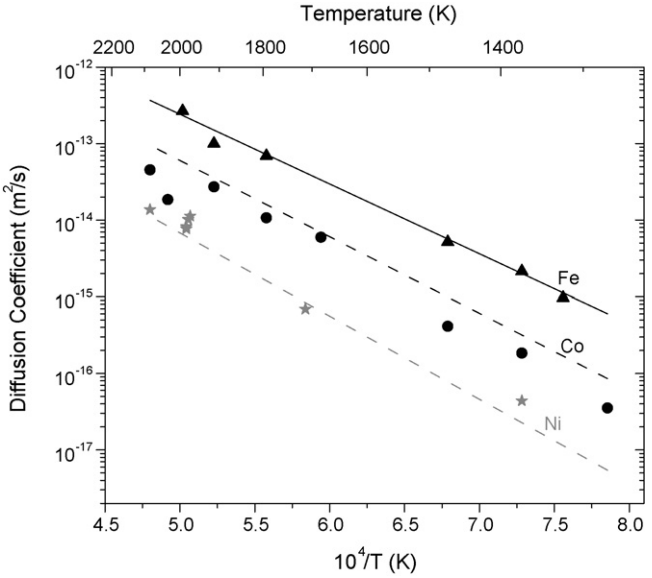

Fig. 14. Arrhenius plot for Fe^{2+}, Co^{2+} and Ni^{2+} diffusion in periclase, with data from Wuensch and Vasilos (1962). The curve for Fe^{2+} is based on the experimental values of D_0 and Q. The curves for Co^{2+} and Ni^{2+} are based on experimental values for D_0, but the values for Q are independent of the experiments, and are predicted from the relation of the migration enthalpy and binding enthalpy to the crystal field stabilization energy as described in the text.

For the divalent transition metals, the experimentally determined activation enthalpy Q in periclase can be taken to represent the sum of the migration enthalpy, H_m, and the enthalpy of binding to an adjacent vacancy, H_b (LeClaire, 1978). Although there is no electrostatic attraction between a divalent transition metal and cation vacancy, there is expected to be an energy cost associated with the presence of a vacancy, as with Cr^{3+}, because it breaks the octahedral symmetry of the site. In the case of the divalent transition metals, the energy cost would be manifested as a positive enthalpy of binding, i.e. a repulsion, between the cation and the vacancy, which would reduce the concentration of vacancies on cation sites that are nearest-neighbors to the divalent transition metal and thus decrease the diffusivity of the transition metal. A prediction of the differences in migration and binding enthalpies among the divalent transition metals can be made, based on our experimental results for Cr^{3+} and Ga^{3+}, if it is assumed that they are proportional to the crystal field stabilization energy. The difference in $CFSE_{oct}$ between Cr^{3+} and Ga^{3+} is 232 kJ/mol, and the differences in migration and binding enthalpies are 24% and 23% of this value, respectively. If the differences in migration and binding enthalpy among the divalent transition metals are also assumed to be 24% and 23% of the difference in $CFSE_{oct}$, the predicted ΔH_m is 17 kJ/mol for Ni^{2+} with respect to Fe^{2+}, and 8.3 kJ/mol for Co^{2+} with respect to Fe^{2+}. Similarly, the predicted ΔH_b would be 16 and 7.9 kJ/mol, respectively. The predicted differences in activation enthalpy, ΔQ, then, are 33 kJ/mol for Ni^{2+} and Fe^{2+} and 16 kJ/mol for Co^{2+} and Fe^{2+}. These predicted values are in reasonable agreement with the measured ΔQ of 28 and 24 kJ/mol, respectively (Wuensch and Vasilos, 1962). Fig. 14 shows that the diffusion data for Co^{2+} and Ni^{2+} are represented fairly well using the experimental values of D_0 and the predicted values of Q, using the experimental Q for Fe^{2+} as a baseline. The crystal field effect thus appears to provide a plausible explanation for the wide range in diffusivity among Ni^{2+}, Co^{2+} and Fe^{2+} in periclase.

4.5. Influence of spin transitions on diffusion in Earth's mantle?

Divalent iron may undergo a transition from a high-spin to a low-spin state in periclase at pressures relevant to Earth's deep mantle (e.g. Badro et al., 2003; Speziale et al., 2005; Sturhahn et al., 2005; Kantor et al., 2006; Tsuchiya et al., 2006; Fei et al., 2007; Lin et al., 2007; Lin and Tsuchiya, 2008). It is possible that other transition metals, which have not yet been studied at high pressure, also undergo high- to low-spin transitions at high pressures. A spin transition in Fe^{2+} involves the transfer of the two unpaired electrons that occupy e_g orbitals to spin-paired t_{2g} orbitals. The transfer of electrons from e_g to t_{2g} orbitals requires energy to pair electrons on the same orbital, but meanwhile lowers the crystal field stabilization energy and the volume (Tsuchiya et al., 2006; Fei et al., 2007) of Fe^{2+} on octahedral sites. As a result, the low-spin state becomes stable at high pressures. The $CFSE_{oct}$ for high-spin Fe^{2+} is approximately $2/5\Delta_0$, where Δ_0 is the crystal field splitting energy between e_g and t_{2g} orbitals, while for low-spin Fe^{2+} $CFSE_{oct}$ is $\sim 12/5\Delta_0$ (Burns, 1993). Similarly, $CFSE_{oct}$ for high-spin Co^{2+} is $4/5\Delta_0$, while for low-spin Co^{2+} the $CFSE_{oct}$ is $9/5\Delta_0$. As discussed above, the diffusion coefficients of transition metal cations in periclase depend strongly on their crystal field stabilization energies, and thus one might expect a significant reduction in diffusivity across a high-spin to low-spin transition. On the other hand, there is also a significant difference in size between low-spin and high-spin Fe^{2+}, unlike the case of Ga^{3+} and Cr^{3+} discussed above, and the influence of this size difference on diffusivity is unconstrained. Also, while Ga^{3+} and Cr^{3+} are present at low concentration, Fe is a major cation in ferropericlase and the spin transition has a significant influence on the thermodynamic and elastic properties of the mineral (Wentzcovitch et al., 2009; Wu et al., 2009). When Fe is in the mixed spin state, any diffusing cation in ferropericlase may have its activation energy barrier lowered due to induction of spin change in neighboring iron atoms arising from stressed bonds at the saddle point (Wentzcovitch et al., 2009). An understanding of the influence of spin transitions on the diffusion properties of ferropericlase requires rigorous calculations and experiments. Below we speculate on the possible magnitude of the effect in terms of the crystal field stabliziation alone.

A crude estimate of the influence of spin transitions on the diffusivity of Fe in periclase can be obtained by extrapolating the

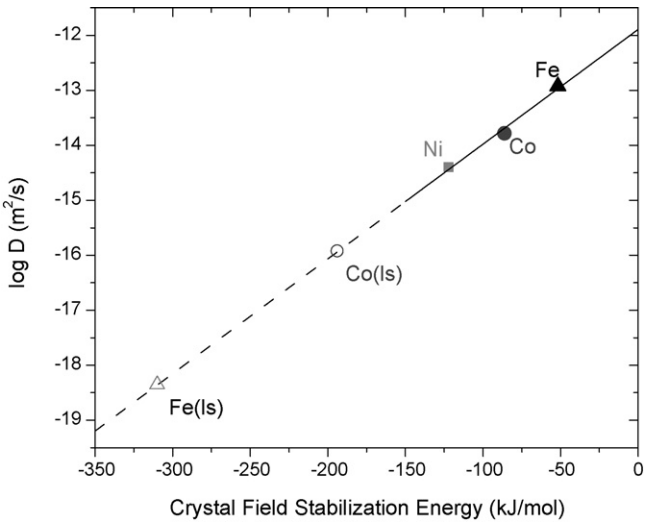

Fig. 15. Diffusion coefficients for divalent transition metal cations in periclase (Wuensch and Vasilos, 1962) at 1600 °C plotted against their crystal field stabilization energies in periclase. A linear extrapolation of the trend to the crystal field stabilization energies estimated for the low-spin states is also shown. In the low-spin state, the relative diffusivities of the divalent transition metals are predicted to reverse, with the diffusion coefficient for low-spin Co^{2+} two orders of magnitude smaller than in the high-spin state, and the diffusion coefficient for low-spin Fe^{2+} five orders of magnitude smaller than in the high-spin state.

trend of diffusivity vs. CFSE observed for the divalent transition metals in periclase to the predicted CFSE for low-spin transition metals (Fig. 15). The crystal field splitting energy Δ_0 for low-spin Fe^{2+} at high pressure appears to be similar to that for high-spin Fe^{2+} at ambient conditions (Keppler et al., 2007), and thus the crystal field stabilization energy for low-spin Fe^{2+} is predicted to be approximately six times the value for high-spin Fe^{2+}, or −310 kJ/mol. Extrapolating along the linear trend shown in Fig. 15, the diffusivity of low-spin Fe^{2+} is predicted to be more than five orders of magnitude lower than for high-spin Fe^{2+}. For Co^{2+} the change in CFSE across the spin transition the diffusion coefficient is predicted to be two orders of magnitude slower in the low-spin than in the high-spin state. There are of course many caveats regarding these estimates, owing to the long extrapolations involved, incomplete understanding of the influence of ionic radius and polarizability (which also change across the spin transition), and in ferropericlase, the influence of the mixed spin state on the diffusion properties (Wentzcovitch et al., 2009). However, despite significant uncertainty regarding the magnitude of the effect, it seems likely that a transition from a high-spin to a low-spin state may significantly reduce the diffusivity of Fe^{2+}, at least in nearly pure periclase. If spin transitions occur in the mantle, they may also significantly reduce the diffusivity of Fe^{3+}, Co^{2+} and Mn^{2+}.

Acknowledgements

We would like to thank Yingwei Fei for opening his lab to us for the piston cylinder experiments, and Chris Hadidiacos for assistance with the electron microprobe analyses. Michelle Weinberger, Andreas Ritzer, Heather Watson, Liz Cottrell, Angele Ricolleau, Li Zhang, Michelle Minitti, and Francis Marino provided invaluable assistance, discussions and hospitality. We would like to thank Renata Wentzcovitch and an anonymous reviewer for constructive comments that improved the paper. This material is based upon work supported by the National Science Foundation under Grant No. 0337125.

References

Badro, J., Fiquet, G., Guyot, F., Rueff, J.P., Struzhkin, V.V., Vanko, G., Monaco, G., 2003. Iron partitioning in Earth's mantle: toward a deep lower mantle discontinuity. Science 300, 789–791.
Balluffi, R.W., Allen, S.M., Carter, W.C., 2005. Kinetics of Materials. John Wiley & Sons, Inc., Hoboken, NJ, 645 pp.
Batra, A.P., Hernandez, J.P., Slifkin, L.M., 1976. Crystal-field effects and the migration of transition-metal ions in AgCl. Phys. Rev. Lett. 36, 876–878.
Batra, A.P., Hernandez, J.P., Slifkin, L.M., 1980. Crystal-field effects in the diffusion of transition-metal ions in silver chloride. Phys. Rev. B 22, 734–742.
Berard, M.F., 1971. Yttrium impurity diffusion in MgO single crystals. J. Am. Ceram. Soc. 54, 58–158.
Burns, R.G., 1993. Mineralogical Applications of Crystal Field Theory, 2nd ed. Cambridge University Press, Cambridge, 551 pp.
Carroll, J.C.G., Corish, J., Henderson, B., Mackrodt, W.C., 1988. Theoretical study of the defect distribution of trivalent cation impurities in MgO. J. Mater. Sci. 23, 2824–2836.
Chakraborty, S., Knoche, R., Schulze, H., Rubie, D.C., Dobson, D., Ross, N.L., Angel, R.J., 1999. Enhancement of cation diffusion rates across the 410-kilometer discontinuity in Earth's mantle. Science 283, 362–365.
Cherniak, D.J., 2003. REE diffusion in feldspar. Chem. Geol. 193, 25–41.
Cherniak, D.J., Watson, E.B., 2003. Diffusion in zircon. Rev. Miner. Geochem. 53, 113–143.
Cherniak, D.J., Zhang, X.Y., Wayne, N.K., Watson, E.B., 2001. Sr, Y, and REE diffusion in fluorite. Chem. Geol. 181, 99–111.
Chick, L.A., Pederson, L.R., Maupin, G.D., Bates, J.L., Thomas, L.E., Exarhos, G.J., 1990. Glycine–nitrate combustion synthesis of oxide ceramic powders. Mater. Lett. 10, 6–12.
Dobson, D.P., Brodholt, J.P., 2000. The electrical conductivity of the lower mantle phase magnesiowüstite at high temperatures and pressures. J. Geophys. Res. 105, 531–538.
Eeckhout, S.G., Bolfan-Casanova, N., McCammon, C., Klemme, S., Amiguet, E., 2007. XANES study of the oxidation state of Cr in lower mantle phases: periclase and magnesium silicate perovskite. Am. Miner. 92, 966–972.
Evans, B., Kohlstedt, D.L., 1995. Rheology of rocks. In: Ahrens, T.J. (Ed.), Rock Physics and Phase Relations: A Handbook of Physical Constants, Ref. Shelf, vol. 3. American Geophysical Union, Washington, DC, pp. 148–165.
Farber, D.L., Williams, Q., Ryerson, F.J., 2000. Divalent cation diffusion in Mg_2SiO_4 spinel (ringwoodite), beta phase (wadsleyite), and olivine: implications for the electrical conductivity of the mantle. J. Geophys. Res. 105, 513–529.
Fei, Y., Zhang, L., Corgne, A., Watson, H., Ricolleau, A., Meng, Y., Prakapenka, V., 2007. Spin transition and equations of state of (Mg, Fe)O solid solutions. Geophys. Res. Lett. 34, L17307, doi:17310.11029/12007GL030712.
Frost, H.J., Ashby, M.F., 1982. Deformation-Mechanism Maps: The Plasticity and Creep of Metals and Ceramics. Pergamon Press, Oxford, 184 pp.
Gautason, B., Muehlenbachs, K., 1993. Oxygen diffusion in perovskite: Implications for electrical conductivity in the lower mantle. Science 260, 518–521.
Gourdin, W.H., Kingery, W.D., 1979. The defect structure of MgO containing trivalent cation solutes: shell model calculations. J. Mater. Sci. 14, 2053–2073.
Hirsch, L.M., Shankland, T.J., 1991. Equilibrium point-defect concentrations in MgO—understanding the mechanisms of conduction and diffusion and the role of Fe impurities. J. Geophys. Res. 96, 385–403.
Hofmann, A.W., 1980. Diffusion in natural silicate melts: a critical review. In: Hargraves, R.B. (Ed.), Physics of Magmatic Processes. Princeton University Press, Princeton, NJ, pp. 385–417.
Hofmann, A.W., Hart, S.R., 1978. An assessment of local and regional isotopic equilibrium in the mantle. Earth Planet. Sci. Lett. 38, 44–62.
Holzapfel, C., Rubie, D.C., Frost, D.J., Langenhorst, F., 2005. Fe–Mg interdiffusion in $(Mg,Fe)SiO_3$ perovskite and lower mantle reequilibration. Science 309, 1707–1710.
Iwamori, H., 1992. Degree of melting and source composition of cenozoic basalts in Southwest Japan: evidence for mantle upwelling by flux melting. J. Geophys. Res. 97, 10983–10985.
Jackson, I., Fitz Gerald, J.D., Faul, U.H., Tan, B.H., 2002. Grain-size-sensitive seismic wave attenuation in polycrystalline olivine. J. Geophys. Res. 107, 2360, doi:2310.1029/2001JB001225.
Kantor, I.Y., Dubrovinsky, L.S., McCammon, C.A., 2006. Spin crossover in (Mg, Fe)O: a Mossbauer effect study with an alternative interpretation of X-ray emission spectroscopy data. Phys. Rev. B 73, 100101.
Karato, S.-i., 1993. Importance of anelasticity in the interpretation of seismic tomography. Geophys. Res. Lett. 20, 1623–1626.
Karato, S.-i., Murthy, V.R., 1997. Core formation and chemical equilibrium in the Earth. I. Physical considerations. Phys. Earth Planet. Int. 100, 61–79.
Karato, S.-i., Wu, P., 1993. Rheology of the upper mantle—a synthesis. Science 260, 771–778.
Keneshea, J.F.J., Fredericks, W.J., 1963. Diffusion of lead ions in potassium chloride. J. Chem. Phys. 38, 1952–1958.
Keppler, H., Kantor, I., Dubrovinsky, L.S., 2007. Optical absorption spectra of ferropericlase to 84 GPa. Am. Miner. 92, 433–436.
Kogiso, T., Hirschmann, M.M., Reiners, P.W., 2004. Length scales of mantle heterogeneities and their relationship to ocean island basalt geochemistry. Geochim. Cosmochim. Acta 68, 345–360.
LeClaire, A.D., 1978. Solute diffusion in dilute alloys. J. Nucl. Mater. 69-70, 70–96.
Lidiard, A.B., 1955. Impurity diffusion in crystals (mainly ionic crystals with the sodium chloride structure). Philos. Mag. 46, 1218–1237.

Lin, J.-F., Tsuchiya, T., 2008. Spin transition of iron in the Earth's lower mantle. Phys. Earth Planet. Int. 170, 248–259.
Lin, J.-F., Vanko, G., Jacobsen, S.D., Iota, V., Struzhkin, V.V., Prakapenka, V.B., Kuznetsov, A., Yoo, C.-S., 2007. Spin transition zone in Earth's lower mantle. Science 317, 1740–1743.
Low, W., 1957. Paramagnetic resonance and optical absorption spectra of Cr^{3+} in MgO. Phys. Rev. 105, 801–805.
Mortlock, A.J., 1968. Divalent cation impurity diffusion in MgO. In: Wachtman, J.B., Franklin, A.D. (Eds.), Mass Transport in Oxides. U.S. Government Printing Office, Washington, DC, pp. 85–87.
Mullen, J.G., 1966. Theory of diffusion in ionic crystals. Phys. Rev. 143, 658–662.
Perkins, R., Rapp, R., 1973. The concentration-dependent diffusion of chromium in nickel oxide. Metall. Mater. Trans. B 4, 193–205.
Qin, Z., 1992. Disequilibrium partial melting model and its implications for trace element fractionations during mantle melting. Earth Planet. Sci. Lett. 112, 75–90.
Ranalli, G., Fischer, B., 1984. Diffusion creep, dislocation creep, and mantle rheology. Phys. Earth Planet. Int. 34, 77–84.
Rubie, D.C., Melosh, H.J., Reid, J.E., Liebske, C., Righter, K., 2003. Mechanisms of metal-silicate equilibration in the terrestrial magma ocean. Earth Planet. Sci. Lett. 205, 239–255.
Saal, A.E., Van Orman, J.A., 2004. The ^{226}Ra enrichment in oceanic basalts: Evidence for melt-cumulate diffusive interaction processes within the oceanic lithosphere. Geochem. Geophys. Geosyst. 5, doi:10.1029/2003GC000620.
Sempolinski, D.R., Kingery, W.D., 1980. Ionic conductivity and magnesium vacancy mobility in magnesium oxide. J. Am. Ceram. Soc. 63, 664–669.
Shannon, R., 1976. Revised effective ionic radii and systematic studies of interatomic distances in halides and chalcogenides. Acta Crystallogr. 32, 751–767.
Shannon, R.D., 1993. Dielectric polarizabilities of ions in oxides and fluorides. J. Appl. Phys. 73, 348–366.
Shewmon, P., 1989. Diffusion in Solids. TMS, Salem, 246 pp.
Solaga, T., Mortlock, A.J., 1970. Concentration dependence of the tracer diffusion of Sc in single crystal MgO. Phys. Status Solidi (a) 3, K247–K250.
Solomatov, V.S., El-Khozondar, R., Tikare, V., 2002. Grain size in the lower mantle: constraints from numerical modeling of grain growth in two-phase systems. Phys. Earth Planet. Int. 129, 265–282.
Speziale, S., Milner, A., Lee, V.E., Clark, S.M., Pasternak, M.P., Jeanloz, R., 2005. Iron spin transition in Earth's mantle. Proc. Natl. Acad. Sci. U.S.A. 102, 17918–17922.
Sturhahn, W., Jackson, J.M., Lin, J.-F., 2005. The spin state of iron in minerals of Earth's lower mantle. Geophys. Res. Lett. 32, L12307, doi:12310.11029/12005GL022802.
Tagai, H., Iwai, S., Iseki, T., Saho, M., 1965. Diffusion of iron, manganese, and chromium oxides into single crystal magnesia. Radex Rundsch 4, 577–583.
Tsuchiya, T., Wentzcovitch, R.M., da Silva, C.R.S., de Gironcoli, S., 2006. Spin transition in magnesiowüstite in Earth's lower mantle. Phys. Rev. Lett. 96, 198501.
Van Orman, J.A., Grove, T.L., Shimizu, N., 2001. Rare earth element diffusion in diopside: influence of temperature, pressure, and ionic radius, and an elastic model for diffusion in silicates. Contrib. Miner. Petrol. 141, 687–703.
Van Orman, J.A., Grove, T.L., Shimizu, N., 2002. Diffusive fractionation of trace elements during production and transport of melt in Earth's upper mantle. Earth Planet. Sci. Lett. 198, 93–112.
Van Orman, J.A., Fei, Y.W., Hauri, E.H., Wang, J.H., 2003. Diffusion in MgO at high pressures: constraints on deformation mechanisms and chemical transport at the core–mantle boundary. Geophys. Res. Lett. 30, 1056, doi:1010.1029/2002GL016343.
Van Orman, J.A., Li, C., Crispin, K.L., 2009. Aluminum diffusion and Al-vacancy association in periclase. Phys. Earth Planet. Int. 172, 34–42.
Watson, E.B., Wark, D.A., Price, J.D., Van Orman, J.A., 2002. Mapping the thermal structure of solid-media pressure assemblies. Contrib. Miner. Petrol. 142, 640–652.
Weber, G.W., Bitler, W.R., Stubican, V.S., 1977. Diffusion of ^{51}Cr in MgO crystals. J. Am. Ceram. Soc. 60, 61–64.
Weber, G.W., Bitler, W.R., Stubican, V.S., 1980. Diffusion of Cr-51 in Cr-doped MgO. J. Phys. Chem. Solid 41, 1355–1359.
Wentzcovitch, R.M., Justo, J.F., Wu, Z., da Silva, C.R.S., Yuen, D.A., Kohlstedt, D., 2009. Anomalous compressibility of ferropericlase throughout the iron spin crossover. Proc. Natl. Acad. Sci. 106, 8447–8452.
Wu, Z., Justo, J.F., da Silva, C.R.S., de Gironcoli, S., Wentzcovitch, R.M., 2009. Anomalous thermodynamic properties in ferropericlase throughout its spin crossover. Phys. Rev. B 80, 014408–014409.
Wuensch, B.J., Vasilos, T., 1962. Diffusion of transition metal ions in single-crystal MgO. J. Chem. Phys. 36, 2917–2922.
Xu, Y., McCammon, C., 2002. Evidence for ionic conductivity in lower mantle $(Mg,Fe)(Si,Al)O_3$ perovskite. J. Geophys. Res. 107, 2251, doi:2210.1029/2001JB000677.
Yager, T.A., Kingery, W.D., 1981. The equilibrium defect structure of iron-doped MgO in the range 600–1200 °C. J. Mater. Sci. 16, 489–494.
Yamazaki, D., Kato, T., Ohtani, E., Toriumi, M., 1996. Grain growth rates of $MgSiO_3$ perovskite and periclase under lower mantle conditions. Science 274, 2052–2054.
Yoshino, T., Watson, E.B., 2005. Growth kinetics of FeS melt in partially molten peridotite: an analog for core-forming processes. Earth Planet. Sci. Lett. 235, 453–468.